

1-1-2017

# Light-Driven Hydrogen Production from Aqueous Solutions Based on a New Dubois-Type Nickel Catalyst

Y. Zhou

*China University of Petroleum*

S. Yang

*Marquette University*

J. Huang

*Marquette University*

---

Accepted version. "Light-Driven Hydrogen Production from Aqueous Solutions Based on a New Dubois-Type Nickel Catalyst," in *Physical Chemistry Chemical Physics*, Vol. 11 (2017). DOI. © 2017 Royal Society of Chemistry. Used with permission.

Marquette University

e-Publications@Marquette

***Chemistry Faculty Research and Publications/College of Arts and Sciences***

***This paper is NOT THE PUBLISHED VERSION; but the author's final, peer-reviewed manuscript. The published version may be accessed by following the link in the citation below.***

*Journal/Monograph*, Vol. xx, No. x (xxxx): XX-XX. [DOI](#). This article is © [publisher] and permission has been granted for this version to appear in [e-Publications@Marquette](#). [publisher] does not grant permission for this article to be further copied/distributed or hosted elsewhere without the express permission from [publisher].

# Light-driven hydrogen production from aqueous solutions based on a new Dubois-type nickel catalyst

Y. Zhou

College of Science, China University of Petroleum (East China), Qingdao, 266580, China  
Department of Chemistry, Marquette University, Milwaukee, Wisconsin

S. Yang

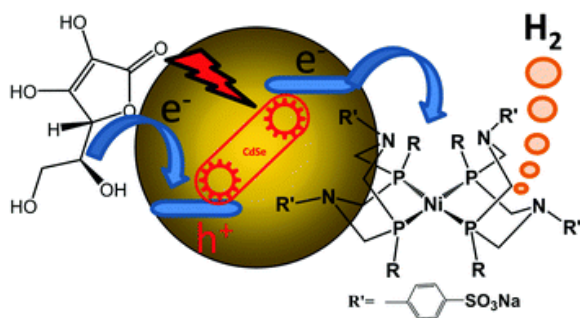
Department of Chemistry, Marquette University, Milwaukee, Wisconsin

J. Huang

Department of Chemistry, Marquette University, Milwaukee, Wisconsin

Abstract

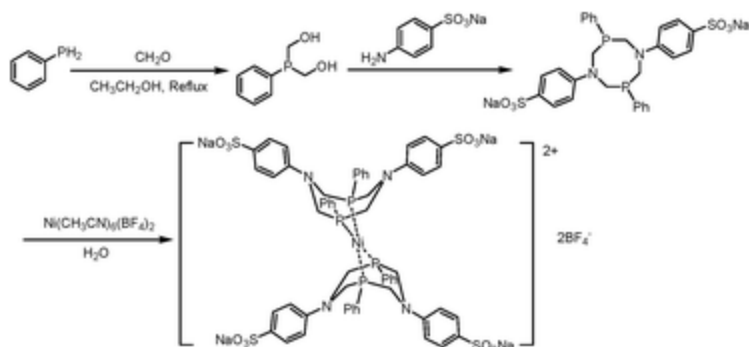
In this work, we report a new photocatalytic system that links multifunctional semiconductor nanocrystals with emerging water-soluble molecular catalysts made of earth-abundant elements for H<sub>2</sub> generation [Ni(P<sub>2</sub><sup>R</sup>N<sub>2</sub><sup>R'</sup>)<sub>2</sub>(BF<sub>4</sub>)<sub>2</sub>]<sup>4-</sup>, R = Ph, R' = [PhSO<sub>3</sub>]<sup>-</sup> (NiS). This noble metal free hybrid exhibits remarkable catalytic activity with a turnover number of 511 for H<sub>2</sub> production and a photon-to-H<sub>2</sub> conversion efficiency of 12.5%. The mechanistic insight into such high efficiency in this photocatalytic system was examined using a combination of steady-state emission and time-resolved absorption spectroscopy.



The photocatalytic generation of H<sub>2</sub> from water requires the efficient coupling of light harvesting materials with hydrogen evolution catalysts (HECs). Since the initial report of the light-driven generation of H<sub>2</sub>,<sup>1,2</sup> different strategies for constructing such photocatalytic systems have evolved. However, these systems typically suffer from significant issues that impact their viability in actual devices. For example, the use of noble metals or metal oxides as catalysts and semiconductor (SC) materials as photosensitizers (PSs) leads to durable catalytic systems that can efficiently catalyze H<sub>2</sub> evolution; yet, their long-term practicality is hampered by the scarcity and high cost of noble metals.<sup>3-7</sup> As a second example, homogeneous catalytic systems composed of synthetic, often bio-inspired, molecular catalysts and molecular PSs have tunable structures and can be readily synthesized.<sup>8-11</sup> However, most of them suffer from photoinstability during prolonged irradiation, in particular, from degradation of the molecular PS.

With a view towards addressing the issues of photocatalyst efficiency, stability, and cost effectiveness, hybrid catalysts that integrate SC nanocrystal PSs and bio-inspired molecular catalysts have emerged as attractive photocatalytic systems for the H<sub>2</sub> evolution reaction (HER).<sup>12-17</sup> In addition to their unique size dependent optical properties, SC nanocrystals have high extinction coefficients across a broad spectral range. Their surfaces can be readily modified to control their solubility in preferred solvents and they are amenable for coupling with specific functional targets in HECs.<sup>18-20</sup> Molecular catalysts that attract particular attention are those that contain active sites with earth-abundant elements.<sup>21,22</sup> To date, the most active synthetic electrocatalyst for the HER is the Ni catalyst developed by Dubois and co-workers, *i.e.*, the bis(1,5-R'-diphospha-3,7-R''-diazacyclooctane) nickel core, [Ni(P<sub>2</sub>R'<sup>N</sup><sub>2</sub>R''<sup>N</sup>)<sub>2</sub>]<sup>2+</sup>,<sup>23-26</sup> and thus is an especially ripe target for further development.

Offering the dual advantages of SC nanocrystal PSs and Dubois-type Ni catalysts, in this work, we developed a new hybrid photocatalytic system that integrates CdSe quantum dots (QDs) with Dubois-type Ni catalysts functionalized with -SO<sub>3</sub><sup>-</sup> groups (NiS, [Scheme 1](#)). The -SO<sub>3</sub><sup>-</sup> group was chosen as the functional group because of its exceptional solubility in H<sub>2</sub>O, which makes NiS water-soluble, thus facilitating light-driven H<sub>2</sub> generation from aqueous solution. Moreover, the synthesis of NiS with the -SO<sub>3</sub><sup>-</sup> group is much more accessible and cost effective compared to its cousin functionalized with -PO<sub>3</sub>H<sub>2</sub>.<sup>26,27</sup> In the presence of ascorbic acid (AA), we demonstrate that this hybrid system can efficiently catalyze the HER in aqueous solution under visible light illumination. Mechanistic studies using emission and time-resolved absorption spectroscopy show that ultrafast charge separation occurs in CdSe QDs through electron transfer (ET) to NiS and hole transfer (HT) to AA.



**Scheme 1** Summary of synthetic procedures of the NiS complex.

NiS was synthesized according to previously published protocols<sup>28</sup> with some modifications ([Scheme 1](#)). Details of the synthesis and structural characterization are provided in the ESI.<sup>†</sup> Briefly, phenylphosphine (330 mg, 3.0 mmol) was added dropwise to a suspension of paraformaldehyde (180 mg, 6.0 mmol) in 5 mL of ethanol under N<sub>2</sub> protection. After refluxing for 12 hours, a solution of sodium salt of sulfanilic acid (586 mg, 3 mmol) in water (2 mL) was added to the mixture. The resulting solution was left overnight with vigorous stirring, after which a white precipitate was isolated. The white precipitate was confirmed to be P<sup>Ph</sup><sub>2</sub>N<sup>C</sup><sub>6</sub>H<sub>4</sub>SO<sub>3</sub>Na<sub>2</sub> by <sup>1</sup>H NMR (Fig. S1, ESI<sup>†</sup>), <sup>31</sup>P NMR (Fig. S2, ESI<sup>†</sup>), <sup>13</sup>C NMR (Fig. S3, ESI<sup>†</sup>) and ESI-MS. The final product, *i.e.* Na<sub>4</sub>[Ni(P<sup>Ph</sup><sub>2</sub>N<sup>C</sup><sub>6</sub>H<sub>4</sub>SO<sub>3</sub>Na)<sub>2</sub>](BF<sub>4</sub>)<sub>2</sub> (NiS), was obtained after mixing 1 eq. of Ni precursor salt ([Ni(CH<sub>3</sub>CN)<sub>6</sub>](BF<sub>4</sub>)<sub>2</sub>) with 2 eq. of the P<sup>Ph</sup><sub>2</sub>N<sup>C</sup><sub>6</sub>H<sub>4</sub>SO<sub>3</sub>Na<sub>2</sub> ligand in H<sub>2</sub>O. The molecular structure of the NiS complex was confirmed by <sup>1</sup>H NMR, <sup>31</sup>P NMR, and elemental analysis.

[Fig. 1a](#) shows the UV-visible absorption spectrum of NiS in H<sub>2</sub>O (red plot). The strong absorption band located at 447 nm can be assigned to the metal-to-ligand charge transfer band from nickel to phosphorus, similar to previously reported Dubois Ni catalysts.<sup>29</sup> [Fig. 1b](#) shows the cyclic voltammogram (CV) of NiS measured in H<sub>2</sub>O solution. The observed two quasi-reversible reduction waves at  $E_{1/2} = -0.558$  V and  $E_{1/2} = -0.817$  V vs. SCE can be assigned to Ni<sup>II/I</sup> and Ni<sup>I/0</sup> redox couples,<sup>26</sup> respectively.

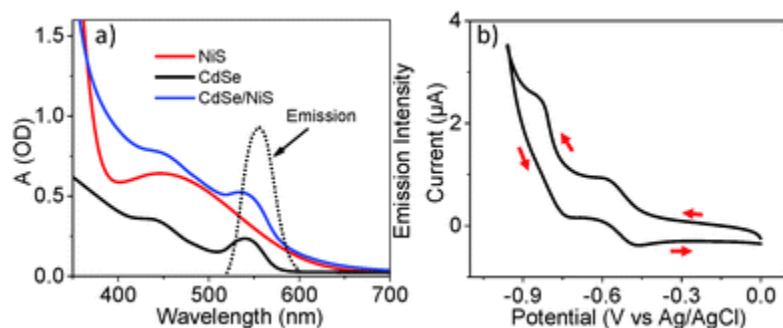


**Fig. 1** (a) UV-visible absorption spectra of NiS, CdSe, and the CdSe/NiS hybrid, and emission spectrum of CdSe in H<sub>2</sub>O. (b) Cyclic voltammogram of NiS measured in H<sub>2</sub>O.

Water soluble CdSe QDs were obtained after ligand exchange of oleic acid capped CdSe QDs with 3-mercaptopropionic acid (MPA), following a previously published procedure<sup>30</sup> (see the ESI<sup>†</sup> for details). The UV-visible absorption spectrum of the synthesized CdSe QDs in H<sub>2</sub>O is also presented in [Fig. 1a](#) (black plot). These QDs have their first exciton band located at 540 nm. According to the model of

Brus,<sup>31,32</sup> the estimated conduction and valence band edges for CdSe QDs (540 nm) are  $-1.14$  V and  $+1.05$  V vs. SCE, respectively. Compared to the 1st and 2nd reduction potentials of the NiS obtained above, the driving forces for the 1st and 2nd ET processes from excited CdSe QDs to NiS are  $-0.582$  eV and  $-0.323$  eV, respectively, suggesting that ET processes from CdSe QDs to NiS in the CdSe/NiS hybrid are thermodynamically feasible.

The photocatalytic performance of the CdSe/NiS hybrid for the HER was evaluated under the illumination of an LED lamp in aqueous solution. Previous studies have shown that the efficiency of light-driven  $H_2$  production is largely dependent on experimental conditions, such as sacrificial donors, proton sources, the pH values of the solution, and the concentrations of the PS and the catalyst.<sup>26,33</sup> Therefore, a series of photocatalytic experiments were carried out by systematically varying these parameters. The initial survey, among AA, lactic acid, and TEOA/TEA, showed that the hybrid system with AA exhibited the highest activity and was thus identified as the most appropriate electron donor and proton source (Fig. S4, ESI<sup>†</sup>). The higher activity in the presence of AA than TEOA/TEA is likely due to the higher acidity of the former than the latter, which is consistent with the pH dependent study discussed below. Meanwhile, the better activity with AA than that with lactic acid can be attributed to the higher oxidation power of AA than lactic acid, which facilitates hole transfer from CdSe QDs to AA. Furthermore, the pH of the AA solution was screened to find the optimum acidity of the solution, from which the solution with pH 3.8 was identified as the best condition for the reaction (Fig. S4, ESI<sup>†</sup>) in terms of activity and durability. The decreased durability for  $H_2$  generation at pH below 3.8 is likely due to more severe corrosion of CdSe QDs under highly acidic conditions.

Using these conditions, the HER rates of the hybrid system as a function of time were measured under illumination of a 505 nm LED lamp (22 mW). Because no appreciable amount of  $H_2$  was observed by omitting AA, NiS or CdSe QDs in the photocatalytic system, all of these components are necessary for the HER. Next, the concentrations of CdSe QDs ( $[CdSe]$ ) and NiS catalysts ( $[NiS]$ ) were systematically varied to obtain the optimum turnover number (TON) for the HER. Fig. 2a shows the time profile of  $H_2$  production measured from solutions with fixed  $[NiS] = 0.2$  mM and variable  $[CdSe]$ . While all samples show notable  $H_2$  generation immediately following illumination, the HER rate varies significantly among these samples. As reflected by the slope of the curves and the overall TON as a function of  $[CdSe]$  (the inset of Fig. 2a), the HER rate initially increases and then decreases with increasing  $[CdSe]$ . Because the maximum TON occurs at  $[CdSe] = 13.7$   $\mu$ M, this QD concentration is used in the subsequent  $[NiS]$  dependence experiments. As shown in Fig. 2b, the TON of the hybrid system increases with decreasing  $[NiS]$  until it reaches its optimum number 511 at  $[NiS] = 0.02$  mM, after which further decrease of  $[NiS]$  slows down the HER rate. These results suggest that the maximum TON (511) has been achieved under the optimized conditions with  $[CdSe] = 13.7$   $\mu$ M and  $[NiS] = 0.02$  mM. Meanwhile, the  $H_2$  generation efficiency of the photocatalytic system after replacing NiS by  $Ni(CH_3CN)_6(BF_4)_2$  is dramatically lower than that of NiS (Fig. S4, ESI<sup>†</sup>), which suggests that NiS is the active species responsible for such a high TON.

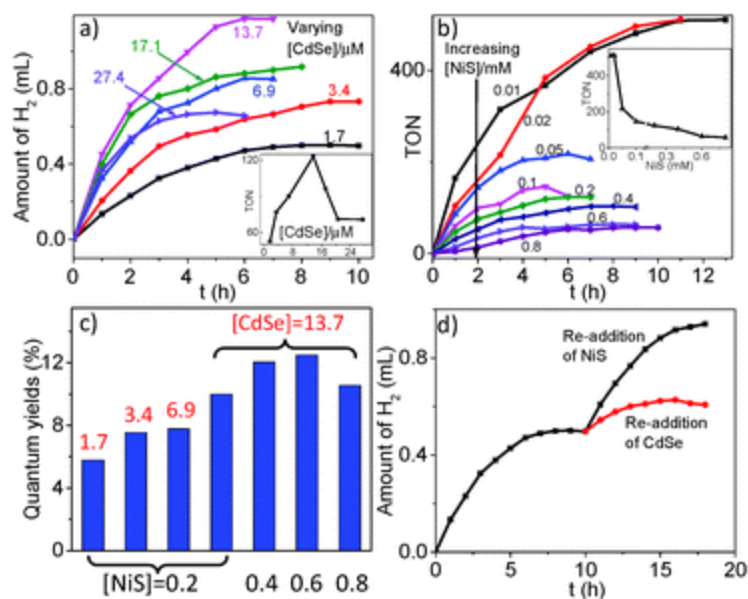


**Fig. 2** Hydrogen evolution profiles of CdSe/NiS hybrids in H<sub>2</sub>O, [AA] = 0.1 M, irradiated at 505 nm (22 mW): (a) effect of varying [CdSe] at [NiS] = 0.2 mM; the inset shows TON as a function of CdSe concentration; (b) effect of varying [NiS] at [CdSe] = 13.7 μM; the inset shows TON as a function of NiS concentration; (c) the estimated photon-to-H<sub>2</sub> quantum yields using various [CdSe] (μM) and [NiS] (mM); and (d) the stability measurements for the HER under optimized conditions.

While the TON against PSs or catalysts is often used to evaluate HER efficiency for a specific photocatalytic system, the direct comparison of efficiencies using TONs among different systems is difficult, as these numbers are largely dependent on the illumination power density. In order to have a valid comparison with previously reported systems, we evaluated the HER efficiency of the CdSe/NiS hybrids in terms of photon-to-H<sub>2</sub> quantum yield. The photon-to-H<sub>2</sub> quantum yield was defined as  $\eta$  (%) =  $\Delta(H_2) \times 2 / \Delta(h\nu) \times 100\%$ , where  $\Delta(H_2)$  is the H<sub>2</sub> generation rate in the first 3 hours and  $\Delta(h\nu)$  is calculated from the power of the incident light (22 mW). Fig. 2c presents the photon-to-H<sub>2</sub> efficiency for samples with different combinations of [CdSe] and [NiS] after 3 h irradiation. Using 0.6 mM of NiS and 13.7 μM of CdSe QDs, we have achieved a photon-to-H<sub>2</sub> efficiency of 12.5%. Although photocatalytic systems based on Ni salts are still benchmarks,<sup>15</sup> and the TON of the current system is lower than several other systems using Dubois Ni catalysts,<sup>26,34,35</sup> the photon-to-H<sub>2</sub> quantum yield observed in the current system compares well with systems using synthetic Ni molecular catalysts in aqueous solution (0.2–15%),<sup>26,27,36–39</sup> largely promising the potential to use this system for solar-to-fuel conversion.

In order to reveal the reasons for the cessation of H<sub>2</sub> generation, NiS and CdSe QDs were alternatively added to an inactive photocatalytic system after 10 h. As shown in Fig. 2d, ~90% of the H<sub>2</sub> generation efficiency is recovered after adding the same amount of NiS, while adding CdSe QDs only recovers a small portion of catalytic activity. These results suggest that the degradation of NiS catalysts is the major limiting factor that leads to the photoinstability of the system though the degradation of CdSe QDs contributes some. To gain more information on how NiS catalysts were degraded, we compared the X-ray absorption near edge structure (XANES) spectra of the catalytic system collected at the Ni-K edge before and after catalysis. As shown in Fig. S5 (ESI<sup>†</sup>), the XANES spectrum before catalysis shows

a prominent pre-edge feature at  $\sim 8336$  eV ( $1s-3d$  transition), while this feature disappeared in the spectrum after catalysis. These results are consistent with previous literature data,<sup>40,41</sup> which can be attributed to the conversion of the NiS geometry from the noncentrosymmetric environment (*i.e.* distorted square planar geometry) to a centrosymmetric environment (octahedral geometry). The octahedral geometry of Ni, together with the negligible edge shift in the XANES spectrum, suggests that the valence state of Ni in the NiS catalyst is believed to remain unchanged ( $\text{Ni}^{\text{II}}$  state) after catalysis, as the  $\text{Ni}^{\text{I}}$  state prefers to have lower coordination. These results together imply that the square planar structure of NiS is essential for its catalytic activity for  $\text{H}_2$  generation.

In addition to the photocatalytic reaction, mechanistic insight into the HER was obtained using a combination of steady state and time-resolved optical spectroscopy. Transient absorption (TA) spectroscopy, a powerful tool for probing exciton dynamics in QDs, was first used to examine the charge separation dynamics in CdSe QDs in the presence of NiS and AA. The sample conditions which give rise to optimum photon-to- $\text{H}_2$  efficiency were used for TA measurements. Fig. 3a shows the femtosecond TA spectra of CdSe QDs after 560 nm excitation. The strong negative feature at 500–550 nm can be assigned to the  $1S$  exciton bleach band, which has been attributed to the reduced oscillation strength of the  $1S(h)-1S(e)$  transition due to the filling of the  $1S(e)$  level upon excitation.<sup>42,43</sup> The bleach band centered at  $\sim 460$  nm and the positive absorption bands at 480 nm and 580 nm can be attributed to the bleach and the Stark-effect induced red shift of the higher absorption bands, respectively, which are typically caused by the presence of  $1S$  excitons.<sup>42</sup> The  $1S$  exciton bleach recovery of CdSe QDs (Fig. 3b), reflecting the electron lifetime in the conduction band of QDs, shows negligible decay within 100 ps, suggesting that multiple excitons are barely generated under the current experimental conditions. In contrast, the  $1S$  exciton bleach recovery in the CdSe/NiS hybrid (Fig. 3b and Fig. S6, ESI<sup>†</sup>) is enhanced compared to that of CdSe, indicating that the  $1S$  electrons in the conduction band of QDs in the CdSe/NiS hybrid are depopulated due to the presence of the NiS catalyst.

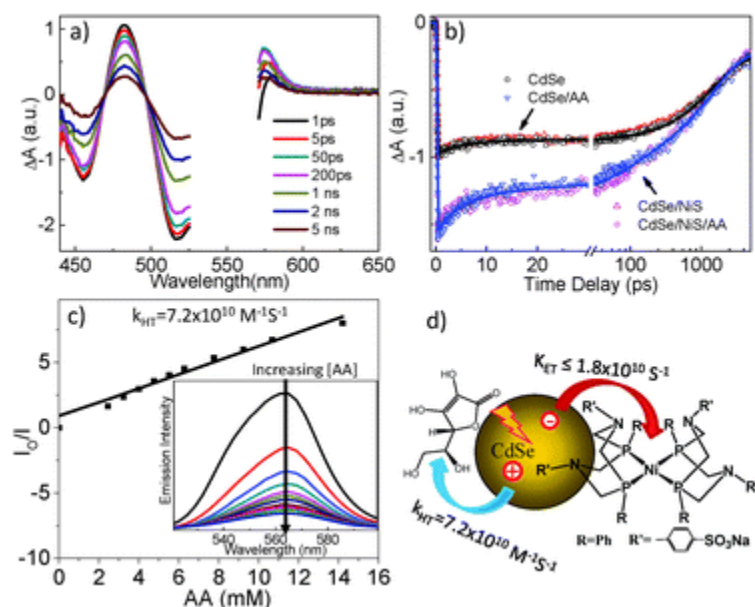


**Fig. 3** (a) Femtosecond absorption spectra of CdSe QDs in  $\text{H}_2\text{O}$  following 560 nm excitation. (b) Comparison of  $1S$  exciton bleach recovery probed at 520 nm for CdSe QDs and CdSe/NiS in the absence

and presence of AA. These kinetics were rescaled by normalizing the amplitude at 5 ns for better comparison of the early time kinetics in the absence and presence of NiS. (c) The Stern–Volmer plot for emission quenching of CdSe QDs by AA. The inset shows the emission spectra of CdSe QDs with different concentrations of AA. (d) Cartoon of charge separation dynamics in CdSe QDs through electron transfer to NiS and hole transfer to AA.

The depopulation dynamics of 1S electrons in the conduction band of CdSe QDs can arise from ET or energy transfer (ENT) to the NiS complex. The ET process results in the formation of a reduced state of NiS while ENT leads to the formation of an excited state of NiS, which in principle can be distinguished by using TA spectroscopy. Unfortunately, due to the extremely small extinction coefficient of NiS ( $\epsilon_{457} = 1160 \text{ cm}^{-1} \text{ M}^{-1}$ ) compared to CdSe QDs ( $\epsilon_{540} = 85\,555 \text{ cm}^{-1} \text{ M}^{-1}$ ),<sup>41</sup> along with the significant overlap between the absorption spectra of CdSe QDs and NiS, it is impossible to identify these species using TA spectroscopy. Instead, we calculated the ENT rate according to the Förster resonant energy transfer (FRET) model,<sup>44</sup> which has been widely used to estimate the ENT rate in various hybrid systems.<sup>45–48</sup> According to this model, the estimated ENT time has an upper limit of 5.5  $\mu\text{s}$ , corresponding to an ENT rate of  $1.8 \times 10^5 \text{ s}^{-1}$  (ESI<sup>†</sup>). Because the ENT rate is much slower than the 1S electron depopulation rate which is  $\sim 1.8 \times 10^{10} \text{ s}^{-1}$  ( $\tau \sim 56 \text{ ps}$ ) obtained from fitting the kinetic traces in Fig. 2b using a previously published model,<sup>20</sup> we attribute the faster exciton bleach recovery in the CdSe/NiS hybrid observed by TA to the ET process. The ET time (56 ps) in the current CdSe/NiS system appears to be fast in terms of bimolecular diffusion interaction. Given that NiS has  $\text{SO}_3^-$  groups which can be used as anchoring groups to nanoparticles,<sup>49</sup> it is highly possible that NiS may have directly attached to the surface of the CdSe QDs, resulting in the ultrafast ET process from CdSe QDs to NiS. In addition, it is notable that the 1S exciton bleach of CdSe/NiS has not fully recovered within our 5 ns time window of the TA experiment (Fig. 3b). Similar uncompleted 1S exciton bleach recovery kinetics in CdSe/molecular adsorbate has been observed previously<sup>43,50</sup> and can be attributed to the presence of free CdSe QDs in the CdSe/NiS solution.

Besides ET from CdSe QDs to the NiS catalyst, understanding the HT dynamics from CdSe QDs to AA is essential for photocatalytic  $\text{H}_2$  generation. Unlike the ET process, which can be measured by probing 1S exciton bleach recovery, HT from CdSe QDs to the hole acceptor, without involving 1S electrons in the conduction band of CdSe QDs, typically has a negligible effect on the 1S exciton bleach recovery of CdSe QDs.<sup>51–53</sup> These results are clearly observed in the current systems, where similar 1S exciton bleach recovery kinetics were observed in the absence and presence of AA for both CdSe QDs and CdSe/Ni samples (Fig. 3b). Alternatively, the HT process can be evaluated by measuring the steady state emission intensity of CdSe QDs as a function of [AA]. It is interesting to note that the initial emission intensity of CdSe QDs increases substantially with increasing [AA] under low [AA] (<0.1 mM) (Fig. S7, ESI<sup>†</sup>). This finding, similar to previously reported data,<sup>54–56</sup> is likely due to the removal of surface trap states due to the addition of AA. Further increase of [AA] (>0.1 mM) results in gradual quenching of the emission intensity of CdSe QDs (inset of Fig. 3c), which can be attributed to HT from CdSe QDs to AA. The HT dynamics can be modeled by the Stern–Volmer equation (Fig. 3c and ESI<sup>†</sup>), from which we obtain the quenching rate constant of  $7.2 \times 10^{10} \text{ M}^{-1} \text{ s}^{-1}$ . Because this quenching rate is relatively large compared to previously reported diffusion controlled systems,<sup>26</sup> it is possible that some AA molecules may have directly associated with CdSe QDs. This also explains the enhanced initial

emission intensity of CdSe QDs upon addition of AA, where AA molecules replaced the surface trap states of QDs.

## Conclusions

In summary, we have developed a new water-soluble hybrid photocatalytic system that integrates a functionalized Dubois-type Ni complex with CdSe QDs. In the presence of ascorbic acid, this system demonstrates a reasonable photon-to-H<sub>2</sub> conversion efficiency compared to other noble-metal free photocatalytic systems based on Ni molecular catalysts. Using steady-state emission and time-resolved absorption spectroscopy, we show that ultrafast charge separation occurs in CdSe QDs through electron transfer to NiS ( $\sim 1.8 \times 10^{10} \text{ s}^{-1}$ ) and hole transfer to AA ( $7.2 \times 10^{10} \text{ M}^{-1} \text{ s}^{-1}$ ). The effective spatial separation of electron-hole pairs in CdSe QDs with electrons in NiS and holes in AA is likely the reason resulting in highly efficient photocatalytic H<sub>2</sub> evolution in this system.

## Acknowledgements

This work was supported by the Marquette University new faculty startup fund and Regular Research Grant. Use of the Advanced Photon Source in the Argonne National Laboratory was supported by the U.S. Department of Energy, Office of Science, and Office of Basic Energy Sciences, under Award No. DE-AC02-06CH11357.

## References

1. A. Fujishima and K. Honda , *Nature*, 1972, **238** , 2
2. J. M. Lehn and J. P. Sauvage , *Nouv. J. Chim.*, 1977, **1** , 3
3. T. Sakata , T. Kawai and K. Hashimoto , *Chem. Phys. Lett.*, 1982, **88** , 50 -54
4. K. P. Acharya , R. S. Khnayzer , T. O'Connor , G. Diederich , M. Kirsanova , A. Klinkova , D. Roth , E. Kinder , M. Imboden and M. Zamkov , *Nano Lett.*, 2011, **11** , 2919 -2926
5. M. Berr , A. Vaneski , A. S. Susha , J. Rodriguez-Fernandez , M. Doblinger , F. Jackel , A. L. Rogach and J. Feldmann , *Appl. Phys. Lett.*, 2010, **97** , 093108
6. L. Amirav and A. P. Alivisatos , *J. Phys. Chem. Lett.*, 2010, **1** , 1051 -1054
7. H. J. Yan , J. H. Yang , G. J. Ma , G. P. Wu , X. Zong , Z. B. Lei , J. Y. Shi and C. Li , *J. Catal.*, 2009, **266** , 165 -168
8. W. R. McNamara , Z. J. Han , P. J. Alperin , W. W. Brennessel , P. L. Holland and R. Eisenberg , *J. Am. Chem. Soc.*, 2011, **133** , 15368 -15371
9. F. Gartner , B. Sundararaju , A. E. Surkus , A. Boddien , B. Loges , H. Junge , P. H. Dixneuf and M. Beller , *Angew. Chem., Int. Ed.*, 2009, **48** , 9962 -9965
10. Z. J. Han , W. R. McNamara , M. S. Eum , P. L. Holland and R. Eisenberg , *Angew. Chem., Int. Ed.*, 2012, **51** , 1667 -1670
11. A. Fihri , V. Artero , A. Pereira and M. Fontecave , *Dalton Trans.*, 2008, 5567 -5569
12. F. Y. Wen and C. Li , *Acc. Chem. Res.*, 2013, **46** , 2355 -2364
13. A. J. Bard and M. A. Fox , *Acc. Chem. Res.*, 1995, **28** , 141 -145
14. P. W. King *Biochim. Biophys. Acta, Bioenerg.*, 2013, **1827** , 949 -957
15. Z. J. Han , F. Qiu , R. Eisenberg , P. L. Holland and T. D. Krauss , *Science*, 2012, **338** , 1321 -1324
16. A. Das , Z. J. Han , M. G. Haghghi and R. Eisenberg , *Proc. Natl. Acad. Sci. U. S. A.*, 2013, **110** , 16716 -16723

17. C. M. Liu , F. Qiu , J. J. Peterson and T. D. Krauss , *J. Phys. Chem. B*, 2015, **119** , 7349 -7357
18. D. V. Talapin , J. S. Lee , M. V. Kovalenko and E. V. Shevchenko , *Chem. Rev.*, 2010, **110** , 389 - 458
19. P. V. Kamat , K. Tvrđy , D. R. Baker and J. G. Radich , *Chem. Rev.*, 2010, **110** , 6664 -6688
20. J. Huang , K. L. Mulfort , P. W. Du and L. X. Chen , *J. Am. Chem. Soc.*, 2012, **134** , 16472 -16475
21. P. A. Jacques , V. Artero , J. Pecaut and M. Fontecave , *Proc. Natl. Acad. Sci. U. S. A.*, 2009, **106** , 20627 -20632
22. P. W. Du , K. Knowles and R. Eisenberg , *J. Am. Chem. Soc.*, 2008, **130** , 12576 -12577
23. J. A. Franz , M. O'Hagan , M. H. Ho , T. Liu , M. L. Helm , S. Lense , D. L. DuBois , W. J. Shaw , A. M. Appel , S. Raugei and R. M. Bullock , *Organometallics*, 2013, **32** , 7034 -7042
24. M. L. Helm , M. P. Stewart , R. M. Bullock , M. R. DuBois and D. L. DuBois , *Science*, 2011, **333** , 863 -866
25. S. Raugei , S. T. Chen , M. H. Ho , B. Ginovska-Pangovska , R. J. Rousseau , M. Dupuis , D. L. DuBois and R. M. Bullock , *Chem. – Eur. J.*, 2012, **18** , 6493 -6506
26. M. A. Gross , A. Reynal , J. R. Durrant and E. Reisner , *J. Am. Chem. Soc.*, 2014, **136** , 356 -366
27. B. C. M. Martindale , G. A. M. Hutton , C. A. Caputo and E. Reisner , *J. Am. Chem. Soc.*, 2015, **137** , 6018 -6025
28. M. D. Doud , K. A. Grice , A. M. Lilio , C. S. Seu and C. P. Kubiak , *Organometallics*, 2012, **31** , 779 -782
29. E. S. Wiedner , J. Y. Yang , S. T. Chen , S. Raugei , W. G. Dougherty , W. S. Kassel , M. L. Helm , R. M. Bullock , M. R. DuBois and D. L. DuBois , *Organometallics*, 2012, **31** , 144 -156
30. W. W. Yu , L. H. Qu , W. Z. Guo and X. G. Peng , *Chem. Mater.*, 2003, **15** , 2854 -2860
31. L. E. Brus *J. Chem. Phys.*, 1983, **79** , 5566 -5571
32. L. E. Brus *J. Chem. Phys.*, 1984, **80** , 4403 -4409
33. P. W. Du , J. Schneider , G. G. Luo , W. W. Brennessel and R. Eisenberg , *Inorg. Chem.*, 2009, **48** , 8646
34. S. C. Silver , J. Niklas , P. W. Du , O. G. Poluektov , D. M. Tiede and L. M. Utschig , *J. Am. Chem. Soc.*, 2013, **135** , 13246 -13249
35. M. P. McLaughlin , T. M. McCormick , R. Eisenberg and P. L. Holland , *Chem. Commun.*, 2011, **47** , 7989 -7991
36. C. A. Caputo , M. A. Gross , V. W. Lau , C. Cavazza , B. V. Lotsch and E. Reisner , *Angew. Chem., Int. Ed.*, 2014, **53** , 11538 -11542
37. J. F. Dong , M. Wang , X. Q. Li , L. Chen , Y. He and L. C. Sun , *ChemSusChem*, 2012, **5** , 2133 - 2138
38. D. H. Wang , Y. W. Zhang and W. Chen , *Chem. Commun.*, 2014, **50** , 1754 -1756
39. H. Kasap , C. A. Caputo , B. C. M. Martindale , R. Godin , V. W. Lau , B. V. Lotsch , J. R. Durrant and E. Reiner , *J. Am. Chem. Soc.*, 2016, **138** , 9183 -9192
40. D. Moonshiram , A. Guda , L. Kohler , A. Picon , S. Guda , C. S. Lehmann , X. Y. Zhang , S. H. Southworth and K. L. Mulfort , *J. Phys. Chem. C*, 2016, **120** , 20049 -20057
41. S. P. Cramer , M. K. Eidsness , W. H. Pan , T. A. Morton , S. W. Ragsdale , D. V. Dervartanian , L. G. Ljungdahland R. A. Scott , *Inorg. Chem.*, 1987, **26** , 2477 -2479
42. H. M. Zhu , N. H. Song and T. Q. Lian , *J. Am. Chem. Soc.*, 2010, **132** , 15038 -15045

43. J. Huang , Z. Q. Huang , Y. Yang , H. M. Zhu and T. Q. Lian , *J. Am. Chem. Soc.*, 2010, **132** , 4858 - 4864
44. T. Förster *Ann. Phys.*, 1948, **437** , 55 -75
45. M. Artemyev , E. Ustinovich and I. Nabiev , *J. Am. Chem. Soc.*, 2009, **131** , 8061 -8065
46. M. Hardzei , M. Artemyev , M. Molinari , M. Troyon , A. Sukhanova and I. Nabiev , *ChemPhysChem*, 2012, **13** , 330 -335
47. K. F. Wu , Z. Y. Chen , H. J. Lv , H. M. Zhu , C. L. Hill and T. Q. Lian , *J. Am. Chem. Soc.*, 2014, **136** , 7708 -7716
48. J. B. Hoffman , H. Choi and P. V. Kamat , *J. Phys. Chem. C*, 2014, **118** , 18453 -18461
49. J. Huang , O. Buyukcakir , M. W. Mara , A. Coskun , N. M. Dimitrijevic , G. Barin , O. Kokhan , A. B. Stickrath , R. Ruppert , D. M. Tiede , J. F. Stoddart , J. P. Sauvage and L. X. Chen , *Angew. Chem., Int. Ed.*, 2012, **51** , 12711 -12715
50. J. Huang , D. Stockwell , Z. Huang , D. L. Mohler and T. Lian , *J. Am. Chem. Soc.*, 2008, **130** , 5632 -5633
51. J. Huang , Z. Q. Huang , S. Y. Jin and T. Q. Lian , *J. Phys. Chem. C*, 2008, **112** , 19734 -19738
52. V. I. Klimov , C. J. Schwarz , D. W. McBranch , C. A. Leatherdale and M. G. Bawendi , *Phys. Rev. B: Condens. Matter Mater. Phys.*, 1999, **60** , R2177 -R2180
53. K. E. Knowles , M. D. Peterson , M. R. McPhail and E. A. Weiss , *J. Phys. Chem. C*, 2013, **117** , 10229 -10243
54. M. D. Peterson , L. C. Cass , R. D. Harris , K. Edme , K. Sung and E. A. Weiss , *Annu. Rev. Phys. Chem.*, 2014, **65**, 317 -339
55. S. Jeong , M. Achermann , J. Nanda , S. Lvanov , V. I. Klimov and J. A. Hollingsworth , *J. Am. Chem. Soc.*, 2005, **127** , 10126 -10127
56. T. C. Kippeny , M. J. Bowers , A. D. Dukes , J. R. McBride , R. L. Orndorff , M. D. Garrett and S. J. Rosenthal , *J. Chem. Phys.*, 2008, **128** , 084713 .

## Footnote

1. † Electronic supplementary information (ESI) available: Description of materials and methods. See DOI: [10.1039/c7cp00247e](https://doi.org/10.1039/c7cp00247e)